Journal of Solid State Chemistry 183 (2010) 1884–1890

Contents lists available at ScienceDirect

Journal of Solid State Chemistry

journal homepage: www.elsevier.com/locate/jssc

Crystal structure and physical properties of the novel ternary intermetallics $URuSi_{3-x}$ and $U_3Ru_2Si_7$

M. Pasturel [a,*], A.P. Pikul [b], M. Potel [a], T. Roisnel [a], O. Tougait [a], H. Noël [a], D. Kaczorowski [b]

[a] Sciences Chimiques de Rennes, Université Rennes 1, UMR CNRS 6226, Campus de Beaulieu, 263 av. Général Leclerc, 35042 Rennes Cedex, France
[b] Institute of Low Temperature and Structure Research, Polish Academy of Sciences, P Nr 1410, 50–950 Wrocław 2, Poland

ARTICLE INFO

Article history:
Received 2 March 2010
Received in revised form
7 June 2010
Accepted 13 June 2010
Available online 19 June 2010

Keywords:
Actinide alloys and compounds
Intermetallics
Magnetically ordered materials
Crystal structure
Heat capacity
Electrical transport
Thermopower

ABSTRACT

Two novel ternary intermediate phases, namely $URuSi_{3-x}$ ($x=0.11$) and $U_3Ru_2Si_7$ were found in the Si-rich part of the U–Ru–Si phase diagram. Single crystal X-ray diffraction measurements, carried out at room temperature, indicated that $URuSi_{3-x}$ crystallizes in its own tetragonal type structure (space group *P4/nmm*, no. 129; unit cell parameters: $a=12.108(1)$ Å and $c=9.810(1)$ Å), being a derivative of the $BaNiSn_3$-type structure. $U_3Ru_2Si_7$ adopts in turn a disordered orthorhombic $La_3Co_2Sn_7$-type structure (space group *Cmmm*, no. 65; unit cell parameters: $a=4.063(1)$ Å, $b=24.972(2)$ Å and $c=4.072(1)$ Å). As revealed by magnetization, electrical resistivity and specific heat measurements, both compounds order magnetically at low temperatures. Namely $URuSi_{3-x}$ is a ferromagnet with $T_C=45$ K, and $U_3Ru_2Si_7$ shows ferrimagnetic behavior below $T_C=29$ K.

1. Introduction

Discovery of coexistence of hidden magnetic order and superconductivity in the heavy fermion compound URu_2Si_2 [1] made the system U–Ru–Si very attractive as possible source of further phases exhibiting unusual physical properties based on their strongly correlated electron behavior, such as heavy fermion, unconventional superconductivity, non-Fermi liquid,…. So far, the existence of quite a few other ternary compounds in that system was reported in the literature, namely: URuSi [2], $U_2Ru_3Si_5$ [3], U_2RuSi_3 [4], U_2Ru_3Si [5], $U_6Ru_{16}Si_7$ [6], $U_2Ru_{12}Si_7$ [7] and URu_3Si_2 [8,9], leaving the Si-rich part of the U–Ru–Si phase diagram quite unexplored. Our systematic investigation of this area revealed the formation of two novel ternary phases, namely $URuSi_{3-x}$ ($x=0.11$) and $U_3Ru_2Si_7$. In the present paper, we report for the first time on their crystal structures, determined by means of single crystal X-ray diffraction, and their basic physical properties, investigated on polycrystalline samples by means of magnetization, specific heat, electrical resistivity and thermoelectric power measurements performed in wide temperature and magnetic field ranges.

2. Experimental details

Polycrystalline samples with the nominal compositions $URuSi_3$ and $U_3Ru_2Si_7$ (with a mass of about 0.5 g each) were prepared by arc melting stoichiometric amounts of the elements (purity above 99.9%) under protective Ti/Zr-gettered argon atmosphere. Homogenization of the products was performed in a high-frequency induction furnace by heating the samples in water-cooled copper crucible up to 1773 ($URuSi_3$) and 1673 K ($U_3Ru_2Si_7$), being close to their melting points, and subsequent slow (about six hours long) cooling down to 1173 and 773 K, respectively. Small single crystals of $URuSi_3$ and $U_3Ru_2Si_7$, suitable for X-ray data collection, were isolated mechanically from the polycrystalline ingots for crystal structure investigations. The remaining parts of the $URuSi_3$ and $U_3Ru_2Si_7$ samples were used for physical properties measurements.

Single crystal X-ray diffraction experiments were performed at room temperature on a four-circle Nonius Kappa CCD diffractometer using Mo $K\alpha$ radiation ($\lambda=0.71073$ Å). Reflections collected on a half Ewald sphere were integrated using the Denzo-Scalepack software [10]. The structures were solved by direct methods using the SIR97 software [11] and refined using the SHELXL-97 software [12] available in the WinGX package [13], after analytical absorption corrections [14].

Quality of the polycrystalline samples of $URuSi_3$ and $U_3Ru_2Si_7$ was checked by means of room temperature X-ray powder

* Corresponding author. Fax: +33 2 23 23 67 99.
E-mail address: mathieu.pasturel@univ-rennes1.fr (M. Pasturel).

0022-4596/$ - see front matter © 2010 Elsevier Inc. All rights reserved.
doi:10.1016/j.jssc.2010.06.008

diffraction (XRD) using an Inel CPS120 diffractometer ($4^\circ \leq 2\theta \leq 116^\circ$) with Cu $K\alpha_1$ radiation ($\lambda = 1.5406$ Å) and chemical analysis, performed on samples embedded in a resin and polished down to 1 μm particle size SiC paper and diamond paste, employing a Jeol JSM 6400 scanning electron microscope equipped with an Oxford 1K EDS spectrometer (SEM–EDS). The two samples were found to be nearly single-phase with the crystal structures corresponding to those determined from the single-crystal data. Small amounts of USi_3 (maximum 10 at%) and Ru_2Si_3 (traces) were established as secondary phases. Since USi_3 is a weak Pauli paramagnet [15] and Ru_2Si_3 is a diamagnet [16,17], it is assumed in the following that the contributions from impurities are negligible in respect to the intrinsic (ferromagnetic) properties of the ternary compounds studied. These contributions are taken into account in the fitting procedure (χ_0 term), and no further corrections were applied to the magnetic data.

Magnetic properties of $URuSi_3$ and $U_3Ru_2Si_7$ were investigated using the Quantum Design MPMS SQUID magnetometer in temperature range 2–300 K and in applied external magnetic fields up to 5 T. Specific heat and electrical resistivity was measured using the Quantum Design PPMS platform in the temperature range from 330 mK up to room temperature, employing a thermal relaxation method [18] and standard four-point technique on bar-shaped samples with spot-welded electrical contacts, respectively. The thermoelectric power, defined as a Seebeck coefficient, was measured from 6 up to 300 K using a homemade equipment with copper as a reference material.

Table 1
Single crystal X-ray diffraction data collection and refinement parameters for $URuSi_{3-x}$ and $U_3Ru_2Si_7$.

Empirical formula	$URuSi_{3-x}$ ($x=0.11$)	$U_3Ru_2Si_7$
Formula weight (g mol^{-1})	420.3	1112.86
Structure type	original	$La_3Co_2Sn_7$
Space group	$P4/nmm$ (no. 129)	$Cmmm$ (no. 65)
Unit cell parameters (Å)	$a=12.108(1)$ $c=9.810(1)$	$a=4.063(1)$ $b=24.972(2)$ $c=4.072(1)$
Unit cell volume (Å^3)	1438.2(2)	413.1(1)
Z/calculated density (g cm^{-3})	18/8.73	2/8.95
Absorption coefficient (mm^{-1})	56.16	63.101
Crystal color and habit	Shiny metallic, plate	Shiny metallic, prism
Crystal size (mm × mm × mm)	0.08 × 0.03 × 0.02	0.03 × 0.03 × 0.09
Theta range	3.16–42.09°	3.26–42.03°
Limiting indices	$-22 \leq h \leq 22$ $-22 \leq k \leq 22$ $-16 \leq l \leq 18$	$-7 \leq h \leq 5$ $-42 \leq k \leq 46$ $-7 \leq l \leq 7$
Collected/unique reflections	33817/2818	4937/882
R(int)	0.127	0.137
Absorption correction	Analytical	Analytical
Max./min. transmission	0.133/0.366	0.101/0.290
Data/restraints/parameters	2818/0/81	882/0/33
Goodness of fit on F^2	1.070	1.064
R indices [$I > 2\sigma(I)$]	$R1=0.045$ $wR2=0.114$	$R1=0.038$ $wR2=0.102$
Extinction coefficient	0.00032(3)	0.0031(4)
Largest difference peak and hole (e Å^{-3})	+7.78 and −7.16	+8.39 and −4.26

3. Results and discussion

3.1. Phase formations

A phase with a chemical composition close to 20U–20Ru–60Si was first observed by SEM–EDS analysis on an arc-melted sample with initial composition 15U–20Ru–65Si, together with the reported binary USi_3 and Ru_2Si_3 and the ternary $U_2Ru_3Si_5$ compounds. Annealing such a sample at high temperature ($\approx$ 1773 K) for 2 h or at low temperature (873 K) for 4 weeks lead to the disappearance of the $U_2Ru_3Si_5$ phase and the strong increase of the 20U–20Ru–60Si phase quantity. This reaction indicates a peritectic formation close in temperature to the liquidus.

The arc-melting of a sample with initial composition 25U–15Ru–Si60 was found to be almost single phase, the only impurity being traces of USi_3. The powder XRD patterns of this sample were similar after arc-melting and annealing for 4 weeks at 873 K, suggesting a congruent melting of the new phase. These patterns were afterwards perfectly indexed with the crystal data obtained from single crystal refinement for $U_3Ru_2Si_7$.

3.2. Crystal structure of $URuSi_{3-x}$

Conditions of the data collection and results of the structure refinement performed on the single crystal isolated from the polycrystalline sample of $URuSi_3$ are summarized in Table 1. The refined atomic coordinates, standardized using STRUCTURE TIDY [19], and equivalent atomic displacement parameters are given in Table 2, and selected interatomic distances are listed in Table 3.

Many rare earth or uranium based ternary compounds with the stoichiometry 1:1:3 (e.g. $UIrSi_3$ [20] or $CeRuSi_3$ [21]), or slightly understoichiometric such as $NdOsSi_{2.85}$ [22], adopt the tetragonal $BaNiSn_3$-type structure with the space group $I4mm$ (no. 107). The crystal structure of $URuSi_{3-x}$ (Fig. 1(a)) is an original type derived from $BaNiSn_3$, with the a and b parameters multiplied by 3 and the c parameter remaining unchanged. The space group found for $URuSi_{3-x}$ is $P4/nmm$ (no. 129). The unit cell contains three non-equivalent sites for uranium atoms (Fig. 1(b)–(d)). The U1 atom (Fig. 2(b)) is surrounded by two regular [Si8] and [Ru4Si4] antiprisms (like in the $BaNiSn_3$-type structure), whereas the antiprisms surrounding the U2 and U3 atoms are irregular. The observed deformations are connected with total or partial substitutions of Ru atoms in Si planes and vice-versa. The refinement of the mixed occupancy of the sites (Ru7/Si7) and (Ru8/Si8) yielded the chemical formula $U_1Ru_{1.0(1)}Si_{2.89(1)}$, i.e. $URuSi_{3-x}$ with $x=0.11$. It should be mentioned that in the final Fourier map there remained five peaks with intensities ranging from 7.8 to 4.8 e Å^{-3}, that is about 10% of the signal expected for a silicon atom. All of them are located at less than 1 Å from the Si atoms present in the distorted part of the structure. This feature likely manifests small crystallographic disorder of Si atoms close to the U2 and U3 atoms, induced by some distortions of the lattice. However, every attempt to include these peaks in the least-square refinement procedure yielded in divergent behavior, probably because of their very small electronic densities. Therefore, they were neglected in the final refinement and the occupancy of the Si9–Si14 sites was assumed to be full.

The X-ray powder diffraction pattern obtained on the sample used for the physical properties measurements is presented in Fig. 2(a) and compared with the theoretical patterns calculated for the new structure type (Fig. 2(b)) or for the classical $BaNiSn_3$-type (Fig. 2(c)). Extra diffraction peaks obtained in the new structure type are clearly visible on the experimental pattern at 20.8° (220), 25.1° (311), 32.3° (322), 37.4° (104), 41.3° (521), 44.7° (531), 45.9° (601) and 53.3° (434), for example, validating our single crystal data (numbers in brackets correspond to the Miller indices of the diffraction peaks). The same results, both on single crystal and powder X-ray diffraction, were obtained after annealing the HF-furnace sample for 3 weeks at 1073 K.

Table 2
Refined atomic coordinates, occupancy rates and equivalent isotropic displacement parameters for $URuSi_{3-x}$ and $U_3Ru_2Si_7$.

	Atom	Wyckoff position	x	y	z	Occupancy rate	Ueq (10^{-3} Å^2)
$URuSi_{3-x}$ (x=0.11)	U1	2*c*	$\frac{1}{4}$	$\frac{1}{4}$	0.7441(1)	1	8(1)
	U2	8*i*	$\frac{1}{4}$	0.5793(1)	0.7463(1)	1	10(1)
	U3	8*j*	0.0856(1)	0.0856(1)	0.2448(1)	1	8(1)
	Ru4	2*a*	$\frac{3}{4}$	$\frac{1}{4}$	0	1	9(1)
	Ru5	2*c*	$\frac{1}{4}$	$\frac{1}{4}$	0.4089(1)	1	10(1)
	Ru6	8*j*	0.5734(1)	0.5734(1)	0.0880(1)	1	8(1)
	Ru7/Si7	8*h*	0.4260(1)	0.5740(1)	$\frac{1}{2}$	0.497(5)/0.503(5)	10(1)
							10(1)
	Si8/Ru8	8*i*	$\frac{1}{4}$	0.6021(2)	0.4206(2)	0.761(6)/0.239(6)	18(1)
							18(1)
	Si9	2*c*	$\frac{1}{4}$	$\frac{1}{4}$	0.1682(5)	1	9(1)
	Si10	8*g*	0.3955(2)	0.6045(2)	0	1	19(1)
	Si11	8*i*	$\frac{1}{4}$	0.0870(2)	0.0087(2)	1	9(1)
	Si12	8*i*	$\frac{1}{4}$	0.0711(3)	0.5038(3)	1	20(1)
	Si13	8*i*	$\frac{1}{4}$	0.5921(3)	0.1745(4)	1	23(1)
	Si14	8*j*	0.0811(1)	0.0811(1)	0.6705(3)	1	12(1)
$U_3Ru_2Si_7$	U1	2*a*	0	0	0	1	9(1)
	U2	4*j*	0	0.3152(1)	$\frac{1}{2}$	1	9(1)
	Ru3	4*i*	0	0.1289(1)	0	0.834(5)	13(1)
	Si3	4*i*	0	0.1289(1)	0	0.166(5)	13(1)
	Si4	2*c*	$\frac{1}{2}$	0	$\frac{1}{2}$	0.834(5)	16(1)
	Si5	4*i*	0	0.2235(2)	0	1	11(1)
	Si6	4*i*	0	0.4149(2)	0	0.834(5)	20(1)
	Si7	4*j*	0	0.4143(2)	$\frac{1}{2}$	0.834(5)	17(1)
	M8 (50% Ru+50% Si)	4*j*	0	0.4350(6)	$\frac{1}{2}$	0.166(5)	22(2)

Table 3
Selected interatomic distances in Å for $URuSi_{3-x}$ and $U_3Ru_2Si_7$.

$URuSi_{3-x}$ (x=0.11)		$U_3Ru_2Si_7$	
U1–4Si14	2.981 (2)	U1–4Si4	2.876 (1)
U1–4Si12	3.201 (4)	U1–4Si6	2.939 (3)
U1–4Si11	3.261 (3)	U1–4Si7	2.954 (3)
U1–4Ru6	3.443 (1)	U1–2U1	4.063 (5)
U1–4U2	3.987 (5)	U1–2U1	4.072 (5)
		U1–8U2	5.437 (5)
U2–2Si14	2.917 (1)	U2–1M8	2.99 (2)
U2–2Si13	2.921 (2)	U2–4Si5	3.034 (2)
U2–1Si12	2.996 (3)	U2–2Si5	3.065 (3)
U2–2Si10	3.064 (2)	U2–4 (Ru3,Si3)	3.197 (1)
U2–2 (Ru8,Si8)	3.188 (2)	U2–2 Si7	3.201 (4)
		U2–2 Si6	3.214 (4)
U2–1U3	4.066 (5)		
U2–2U2	4.134 (5)		
U3–1Si9	2.913 (2)	Ru3–2Si7	2.304 (2)
U3–1Si14	2.974 (2)	Ru3–2Si6	2.307 (2)
U3–2Si13	3.012 (2)	Ru3–1Si5	2.363 (4)
U3–2Si11	3.054 (2)		
U3–1Ru6	3.128 (1)	M8–2Si3	3.29 (2)
U3–2(Ru7,Si7)	3.166 (1)	M8–4U1	3.30 (2)
U3–1Si12	3.232 (2)		
(Ru8,Si8)–1Si12	2.250 (4)	Si5–2Si5	2.425 (4)
(Ru8,Si8)–2(Ru7,Si7)	2.294 (2)		

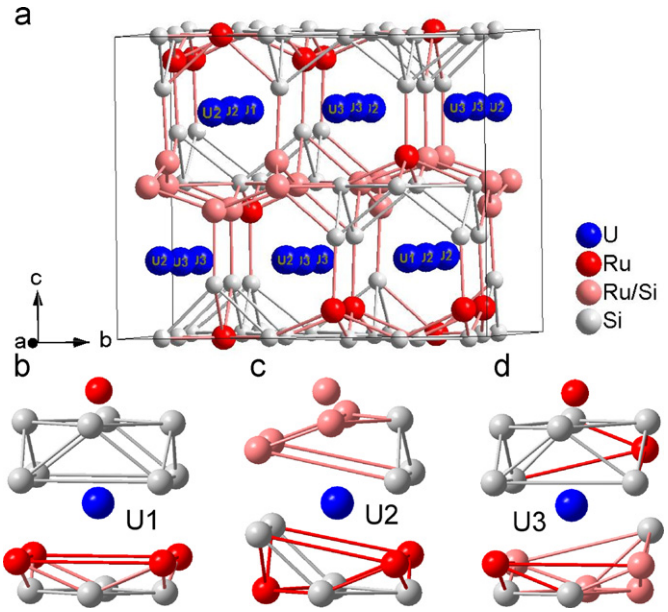

Fig. 1. (a) Crystal structure of $URuSi_{3-x}$ and coordination spheres of (b) U1-, (c) U2- and (d) U3-atoms.

Despite the mixed occupancy of the sites (Ru7/Si7) and (Ru8/Si8), EDX spectroscopy on samples with compositions around U:Ru:Si of 1:1:2.89 does not clearly show (i.e. within the 1 at% error bar of the instrument) any homogeneity domain for this phase.

It is worthwhile to note that the shortest U–U distances are about 4.0 Å, i.e. they are smaller than in the antiferromagnet $UIrSi_3$ (4.17 Å) [20], yet considerably larger than the Hill criterion for U atoms (3.5 Å). Hence, one may expect that U-atoms in $URuSi_3$ may carry a localized magnetic moment.

3.3. *Crystal structure of $U_3Ru_2Si_7$*

Table 1 summarizes the data collection conditions and the structure refinement results. The collected reflections were indexed with the orthorhombic space-group *Cmmm* (no. 65) and

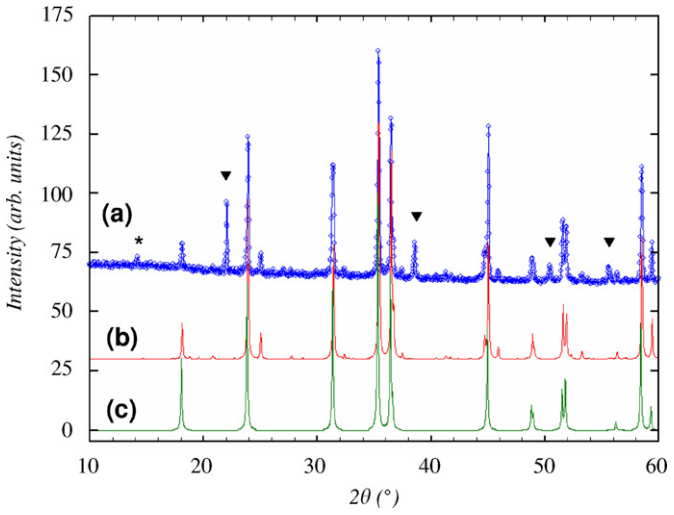

Fig. 2. X-ray powder diffraction patterns (a) experimentally measured, (b) calculated for the structure obtained by single crystal X-ray diffraction and (c) calculated for the classical $BaNiSn_3$ structure type. (*) symbol indicates a sample holder peak and (B) symbols the peaks attributed to USi_3 (space-group $Pm\bar{3}m$, $a=4.036$ Å). For clarity, Ru_2Si_3 peaks are not marked due to their extremely small intensity.

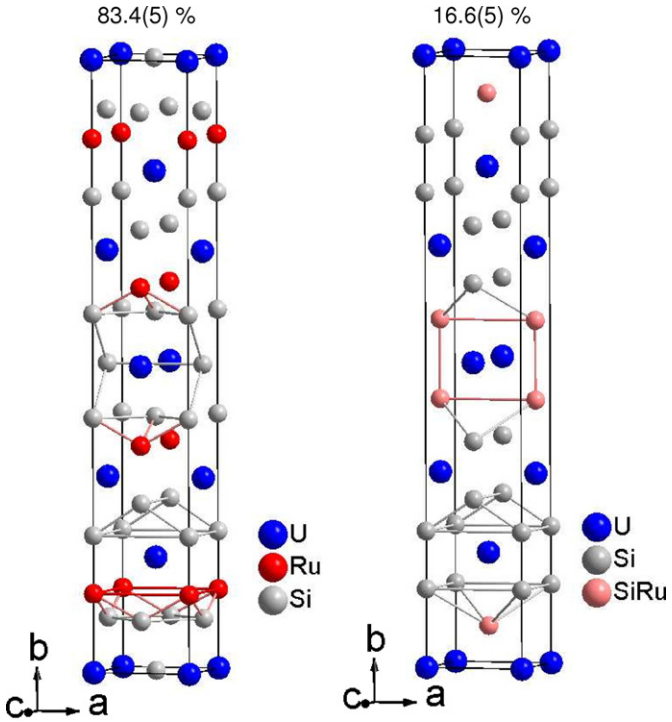

Fig. 3. Decomposed crystal structure of $U_3Ru_2Si_7$ obtained by single crystal X-ray diffraction. A statistical distribution of both cells is assumed in the crystal, according to the indicated percentages.

unit cell parameters $a=4.063(1)$ Å, $b=24.972(2)$ Å and $c=4.072(1)$ Å (Table 1). These data are compatible with the $La_3Co_2Sn_7$ structure type already reported for $U_3Fe_2Si_7$, $U_3Co_2Si_7$ [23] and $U_3Co_2Ge_7$ [24]. Structure resolution allowed localizing seven atomic sites (2 uranium, 1 ruthenium and 4 silicon atoms) and their atomic positions usually met in this structure type. Nevertheless, despite a reasonable value of the mosaïcity of the crystal ($\sim$0.924(3)°), the structure refinement did not lead to satisfying reliability factors. First of all, the equivalent thermal displacement parameter of the ruthenium on the 4*i* site was too high, indicating a too large calculated electron density on this site. Two hypotheses were attempted for this site: (i) a partial occupancy by Ru only or (ii) a full but Ru/Si mixed occupancy. Then, somewhat high equivalent thermal displacement parameters were observed for Si-atoms located at 2*c* (Si4), 4*i* (Si6) and 4*j* (Si7), indicating partial occupancies of these sites. Finally, a remaining peak with quite high intensity ($\sim$16 eÅ^{-3}) was found in the Fourier map at a 4*j* site (*M*8) located at 1.63 Å from one Si4 atom and 2.09 Å from two Si6 and two Si7 atoms. Hypotheses of carbon or oxygen atoms located at this 4*j* position were rejected for different considerations: (i) Si–C distances would be too small compared with those observed in covalent cubic or hexagonal SiC [25] and (ii) O atom is expected to occupy a site close to an U atom rather than between five Si atoms [26]. Considering literature data, such a 4*j* position is mixed occupied by Ni/Si while the *2c* site is empty in $RE_3Ni_{2+x}Si_{8-x}$ (*RE*=La, Ce) [27,28]. This is the only difference between $Ce_3Ni_2Si_8$ and $La_3Co_2Sn_7$ structure types, with the unit cell parameters being nearly identical in both structures. Interatomic distances between M8 and Si4, Si6 and Si7 are too close to be simultaneously occupied. Thus, a model in which the occupancy of *M*8 site must be equal (i) to the deficiency on the Si4, Si6 and Si7 sites and (ii) to the deficiency or mixed occupancy on the 4*i* Ru3 site was assumed (Table 2). The best reliability factors and trustable equivalent thermal displacement parameters were obtained for a *M*8 atom composition arbitrary fixed to 50% Si–50% Ru (other compositions were tested but gave worse results) and mixed Ru/Si occupancy of the Ru3 4*i* site. "$U_3Ru_2Si_7$" compound can then be described as a mixed crystal build with statistical superposition of two different crystal structures (Fig. 3). The first one, where the 4*i* Ru3 site is fully occupied by ruthenium atoms, perfectly fits with the $La_3Co_2Sn_7$ structure type with full occupancy of 2*c*, 4*i* and 4*j* sites by Si4, Si6 and Si7, respectively. The second structure keeps the same space-group, cell parameters, U1, U2 and Si5 skeleton, but the substitution of Si for Ru on the 4*i* Ru3 site is accompanied by full occupancy of the 4*j* *M*8 site by 50%Ru–50%Si and emptiness of 2*c* (Si4), 4*i* (Si6) and 4*j* (Si7) sites, thus showing features of the $CeNi_{2+x}Si_{8-x}$ structure type. Refinement of the occupancy rate was performed using SHELXL-97 considering a "mean structure" of the two previous ones. It converges to a 83–17 at% ratio between both phases, respectively. Notice, this refinement assumes a statistical distribution of both kind of cell in the crystal. Further experiments, using high resolution transmission electron microscopy for example, are planned to confirm this hypothesis or to observe any segregation of the second type inside the $La_3Co_2Sn_7$ type matrix.

No clear explanation arises to explain the disordered structure of this silicide. A reason might arise from the high-frequency furnace heat-treatment applied to the sample but crystals obtained after arc-melting or after annealing at 1073 K for three weeks exhibit the same disordered structure. Substitutions or vacancies mechanisms are nevertheless observed in structures such as $La_3Ni_{2+x}Si_{8-x}$, $Ce_3Ni_{2+x}Si_{8-x}$ [28] or $Ce_3Ni_{2-x}Sn_{7-y}$ [29], which are clearly related to $U_3Ru_2Si_7$.

Refinement of occupancy rates of such a mixed structure lead to a global chemical formula close to $U_3Ru_{1.83}Si_{6.67}$, i.e. characteristic of a slightly Ru and Si deficient structure. SEM–EDS analyses cannot distinguish between this latter composition and the $U_3Ru_2Si_7$ one, because they are within the 1 at% precision of the measurement. Nevertheless, a solubility domain is observed, ranging from $U_3Ru_2Si_7$ to $U_3Ru_{1.5}Si_{7.5}$, which can occur due to the vacancy/substitution mechanisms on Ru and Si sites.

3.4. *Physical properties of $URuSi_{3-x}$ and $U_3Ru_2Si_7$*

Figs. 4 and 5 present the temperature dependencies of the inverse magnetic susceptibility, $\chi^{-1}(T)$, measured for

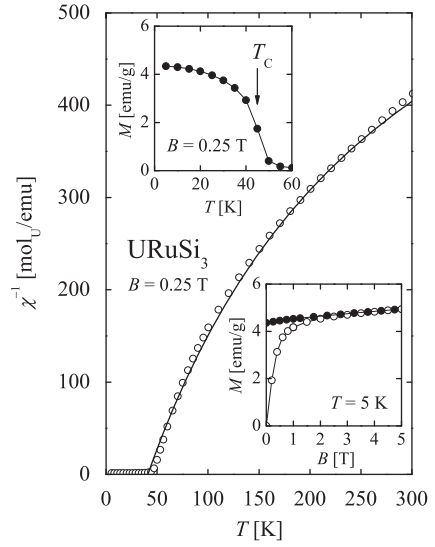

Fig. 4. Temperature dependence of the inverse magnetic susceptibility of $URuSi_{3-x}$. Solid line is a fit of Eq. (1) to the experimental data. Upper inset: low-temperature magnetization of $URuSi_{3-x}$, measured in field-cooling regime; thin solid curve serves as a guide for the eyes and the arrow marks the ordering temperature. Lower inset: isothermal magnetization of $URuSi_{3-x}$ measured as a function of increasing (open symbols) and decreasing (closed symbols) external magnetic field; thin solid lines serve as a guide for the eyes.

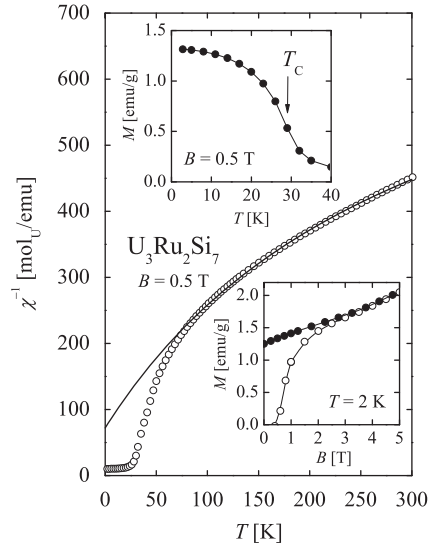

Fig. 5. Inverse magnetic susceptibility of $U_3Ru_2Si_7$ as a function of temperature. Solid line is a fit of the Curie–Weiss law (Eq. (1)) to the experimental data. Upper inset: magnetization of $U_3Ru_2Si_7$ measured as a function of temperature in field-cooling regime; thin solid line serves as a guide for the eyes and the arrow marks temperature of a magnetic ordering. Lower inset: isothermal magnetization of $U_3Ru_2Si_7$ measured as a function of increasing (open circles) and decreasing (closed circles) external magnetic field; thin solid curves serve as a guide for the eyes.

polycrystalline $URuSi_{3-x}$ and $U_3Ru_2Si_7$ samples, respectively, calculated per mole of U atoms. For the first compound $\chi^{-1}(T)$ can be described in the temperature range 60–300 K by the modified Curie–Weiss law [30]

$$\chi(T) = \frac{1}{8}\frac{\mu_{\mathrm{eff}}^2}{(T-\theta_p)} + \chi_0 \qquad (1)$$

where μ_{eff} is the effective magnetic moment, θ_p the Weiss constant and χ_0 a sum of the temperature independent contributions, e.g. Pauli paramagnetism of conduction-band electrons, core diamagnetism, Van Vleck paramagnetism, etc. The parameters derived by least-squares fitting of Eq. (1) to the experimental data are as follows: $\mu_{\mathrm{eff}}=1.60(2)\,\mu_B$, $\theta_p=41(1)$ K and $\chi_0=12.5(3)\times10^{-4}$ emu/mol$_U$ for $URuSi_{3-x}$. The strongly reduced value of the effective magnetic moment (much lower than the theoretical ones calculated for free U^{3+} (3.62 μ_B) and U^{4+} (3.58 μ_B) ions assuming a Russel–Saunders coupling) might result from crystal field interactions but the magnitude of this reduction rather suggest that either not all U atoms in $URuSi_3$ carry magnetic moments (there are three non-equivalent U positions in the unit cell—Fig. 1) or the magnetism in this compound has an itinerant nature. The latter hypothesis seems supported by the relatively large value of χ_0. In turn, the positive Weiss constant indicates strong ferromagnetic correlations, which give rise to a ferromagnetic ordering at low temperatures with T_C being very close to θ_p (see below).

In the case of $U_3Ru_2Si_7$ the susceptibility data (Fig. 5) can be approximated by Eq. (1) in the interval 80–300 K only. The so-derived parameters are $\mu_{\mathrm{eff}}=1.64(2)\,\mu_B$, $\theta_p=-27(3)$ K and $\chi_0=1.19(2)\times10^{-3}$ emu/mol$_U$. Although the reduced value of μ_{eff} and the strongly enhanced magnitude of χ_0 suggest itinerant magnetism scenario also for this compound, the negative θ_p hints at predominance of antiferromagnetic-like interactions. Actually, the behavior of $\chi^{-1}(T)$ displayed in Fig. 5 is characteristic of ferrimagnetic systems. An obvious reasoning for possible ferrimagnetism in $U_3Ru_2Si_7$ is the presence of two sublattices of uranium atoms (see Fig. 3).

As can be inferred from the insets of Figs. 4 and 5, $URuSi_{3-x}$ and $U_3Ru_2Si_7$ order magnetically below 45 and 29 K, respectively. Characteristic shapes of the $M(T)$ and $M(H)$ dependencies are consistent with the ferromagnetic-like character of both phases. In $URuSi_3$ the magnetization measured at 5 K nearly saturates in a field of 5 T and the ordered magnetic moment calculated per formula unit reaches about 0.37 μ_B. The magnetic remanence is 4.36 emu/g. For $U_3Ru_2Si_7$ one observes at 2 K a pronounced quasi-linear rise of the magnetization in strong fields, reminiscent of the behavior of ferrimagnets. The magnetic moment calculated per formula unit is only 0.42 μ_B in 5 T, while the remanent magnetization is equal to 1.25 emu/g. The reduced values of the magnetic moments support the presumption on the itinerant character of the magnetism in both compounds.

The specific heat data of $URuSi_{3-x}$ and $U_3Ru_2Si_7$ are shown in Fig. 6. The ratio $C(T)/T$ exhibits a pronounced peak at $T_C=45$ K for $URuSi_{3-x}$ and a much less resolved anomaly at $T_C=29$ K for $U_3Ru_2Si_7$. At the lowest temperatures, i.e. in the range 350 mK–10 K, the $C(T)/T$ curves follow the relation [31]:

$$C(T) = \gamma T + \frac{12}{5}\pi^5\frac{rR}{\theta_D^3}T^3 \qquad (2)$$

where the first term describes the electronic contribution to the specific heat (with the Sommerfeld coefficient γ) and the second term represents the heat capacity of phonons within a low-temperature limit of the Debye model (with the gas constant R, the number of atoms per formula unit r and the characteristic Debye temperature Θ_D). Least-squares fitting of Eq. (2) to the experimental data (solid lines in the insets of Fig. 6) yielded $\gamma=47$ mJ/(mol K^2) and $\Theta_D=325$ K for $URuSi_{3-x}$, and $\gamma=297$ mJ/(mol K^2) and $\Theta_D=267$ K for $U_3Ru_2Si_7$. The obtained values of the Debye temperatures are typical for U-based intermetallic compounds. The Sommerfeld coefficient derived for $URuSi_{3-x}$ is rather small if one considers that there are as many as three U atoms in the unit cell. The γ coefficient found for $U_3Ru_2Si_7$ is considerably larger: with three U atoms in the formula unit and two U atoms in the unit cell it yields an average value of about 50 mJ/(mol K^2) per U atom. This slightly enhanced electronic term

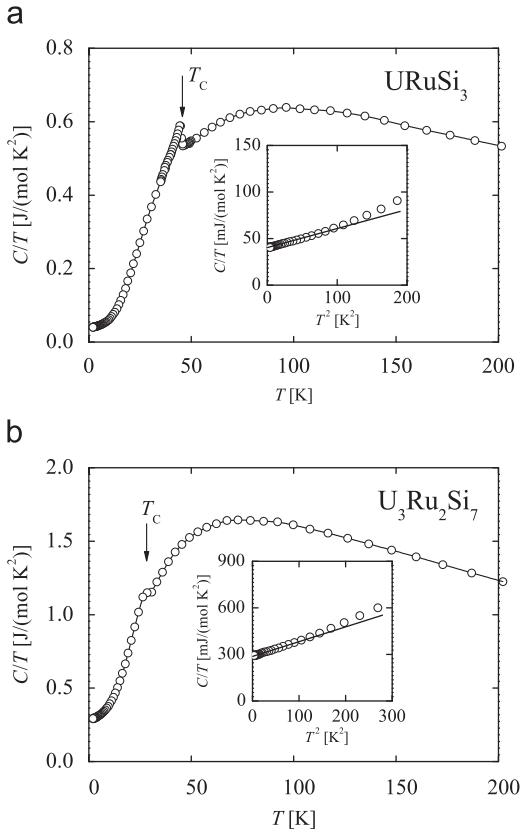

Fig. 6. Specific heat of $URuSi_{3-x}$ (a) and $U_3Ru_2Si_7$ (b) divided by temperature as a function of T; thin solid lines serve as a guide for the eyes. The arrows mark temperatures of magnetic phase transitions. The insets: C/T as a function of squared temperature; thick solid lines are fittings of Eq. (2) to the experimental data.

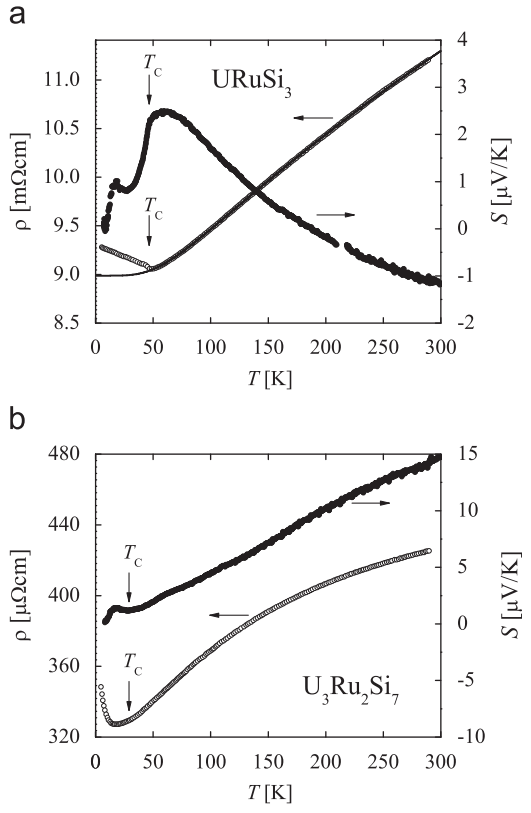

Fig. 7. Temperature variations of electrical resistivity (open symbols) and thermoelectric power (closed symbols) measured for $URuSi_{3-x}$ (a) and $U_3Ru_2Si_7$ (b) in zero magnetic field. The arrows mark the ordering temperatures deduced from other physical-properties measurements.

in the specific heat might manifest the presence of some Kondo interactions, which possibly contribute also the electrical transport in this compound.

The temperature dependencies of the electrical resistivity and the thermoelectric power of $URuSi_{3-x}$ and $U_3Ru_2Si_7$ are presented in Fig. 7. In the paramagnetic region, both compounds exhibit metallic-like character of the electrical conduction. The large magnitude of the resistivity of the former compound is likely caused by considerable structural disorder in its unit cell with mixed Ru/Si occupancies on two specific atomic sites. In turn, the room temperature value of the resistivity of $U_3Ru_2Si_7$ is of the order usually observed for U-based intermetallics, yet it decreases only a little with decreasing temperature. This behavior may be also attributed to high degree of structural disorder associated with the vacancies on most of the Si positions and mixed Ru/Si occupancy on one of the sites.

Assuming the validity of the Matthiessen rule, the resistivity of intermetallics can often be analyzed in terms of the Bloch–Grüneissen–Mott (BGM) formula [32]

$$\rho(T) = (\rho_0 + \rho_0^{\infty}) + 4RT\left(\frac{T}{\Theta_D}\right)^4 \int_0^{\Theta_D/T} \frac{x^5 dx}{(e^x-1)(1-e^{-x})} - KT^3 \qquad (3)$$

where $(\rho_0+\rho_0^{\infty})$ stands for the sum of the residual resistivity due to static defects in the crystal lattice and the spin-disorder resistivity due to the presence of disordered magnetic moments, respectively, the second term describes the phonon contribution to the total resistivity, and the third one represents s–d interband scattering processes. For $URuSi_{3-x}$ least-squares fitting Eq. (3) to the experimental data in the range 40–300 K yielded the parameters: $\rho_0+\rho_0^{\infty}=8.99(5)$ mΩcm, $\Theta_D=345(2)$ K, $R=8.74(4)$ mΩcm/K and $K=4.78(3)\times10^{-6}$ mΩcm/K^3. Worth noting is that the so-derived value of the Debye temperature is very close to that obtained in the analysis of the specific heat thus supporting appropriateness of the approach. On the contrary, the formula given in Eq. (3) appeared to be insufficient for describing the resistivity of $U_3Ru_2Si_7$ in any extended temperature region with reasonable values of the parameters. Clearly, it is because of strongly curved character of the $\rho(T)$ dependence, presumably indicating strong contribution due to spin fluctuations.

For both compounds the resistivity exhibits an upturn below the respective Curie temperature. In the case of ferrimagnetic $U_3Ru_2Si_7$ this feature likely manifests the formation of "magnetic" Brillouin zone inside the "chemical" one. In turn, for $URuSi_3$ no such explanation seems applicable, unless more complex magnetic ordering than simple ferromagnetism is involved. Another possible origin of the observed behavior may be somehow related to the structural disorder.

The thermoelectric power, $S(T)$, of $URuSi_{3-x}$ is very small. At room temperature it amounts to -1.2 μV/K, becomes positive below 190 K and forms a broad maximum near 60 K where it reaches only +2.5 μV/K. The ferromagnetic phase transition manifests itself in the $S(T)$ curve as a distinct kink at $T_C=45$ K, followed by rapid decrease at lower temperatures. At about 16 K another small local maximum occurs, below which the thermoelectric power decreases towards zero. In turn, the thermopower of $U_3Ru_2Si_7$ is positive in the whole temperature range studied. At room temperature it is +15 μV/K, i.e. more than 12 times larger than in $URuSi_{3-x}$. Upon lowering the temperature S decreases nearly linearly. At the Curie temperature $T_C=29$ K a shallow minimum in the $S(T)$ curve is visible, and near 16 K a small maximum occurs.

4. Conclusions

Two novel intermetallic phases have been discovered to form in the U–Ru–Si ternary system, namely $URuSi_{3-x}$ ($x=0.11$) and $U_3Ru_2Si_7$. Single-crystal X-ray diffraction indicated that $URuSi_{3-x}$ crystallizes in a new tetragonal structure type derived from the $BaNiSn_3$-type, while $U_3Ru_2Si_7$ adopts a disordered orthorhombic $La_3Co_2Sn_7$-type. Both crystal structures present much structural disorder associated with mixed and/or deficient occupancies of some crystallographic sites. Further crystallographic studies, for example by high resolution transmission electron microscopy or neutron diffraction are envisaged to discover if any long range order exists for the substitutions and vacancies. Magnetization, specific heat and electrical resistivity measurements have revealed that $URuSi_{3-x}$ orders ferromagnetically at $T_C=45$ K, whereas $U_3Ru_2Si_7$ is probably ferrimagnetic below $T_C=29$ K. Some characteristic features in the bulk properties hint at an itinerant character of the magnetism in both compounds. Further experimental studies are necessary to check the latter presumption, some of which are presently underway.

Acknowledgments

The authors are grateful to Sandra Casale and Isabelle Péron (CMEBA, Université Rennes1) for SEM–EDX analyses and to Dariusz Badurski for his assistance in electrical resistivity measurements. This work was partially supported by the French–Polish Integrated Activity Program "Polonium" no. 14241TM.

Appendix. Supplementary materials

Supplementary data associated with this article can be found in the online version at doi:10.1016/j.jssc.2010.06.008

References

[1] T.T.M. Palstra, A.A. Menovsky, J. van den Berg, A.J. Dirkmaat, P.H. Kes, G.J. Nieuwenhuys, J.A. Mydosh, Phys. Rev. Lett. 55 (1985) 2727–2730.
[2] R. Troć, V.H. Tran, J. Magn. Magn. Mater. 73 (1988) 389–397.
[3] E. Hickey, B. Chevalier, P. Gravereau, J. Etourneau, J. Magn. Magn. Mater. 90–91 (1990) 501–502.
[4] R. Pöttgen, P. Gravereau, B. Darriet, B. Chevalier, E. Hickey, J. Etourneau, J. Mater. Chem. 4 (3) (1994) 463–467.
[5] A. Vernière, P. Lejay, P. Bordet, J. Chenavas, J.P. Brison, P. Haen, J.X. Boucherle, J. Alloys Compd. 209 (1994) 251–255.
[6] P. Lejay, A. Vernière, J.X. Boucherle, G. André, Physica B 206–207 (1995) 522–524.
[7] A.V. Zelinskiy, O.I. Bodak, V.M. Davydov, H. Noël, P. Rogl, Yu.D. Seropegin, in: Proceedings of the Eighth Conference on Crystal Chemistry of Intermetallic Compounds, L'viv, Ukraine, 25–28 September 2002.
[8] H. Barz, Mat. Res. Bull. 15 (1980) 1489–1491.
[9] U. Rauchschwalbe, U. Gottwick, U. Ahlheim, H.M. Mayer, F. Steglich, J. Less-Common Met. 111 (1985) 265–275.
[10] Z. Otwinowski, W. Minor, Processing of X-ray diffraction data collected in oscillation mode, methods in enzymology, in: C.W. Carter Jr., R.M. Sweet (Eds.), Macromolecular Crystallography, Part A, vol. 276, Academic Press1997, pp. 307–326.
[11] A. Altomare, M.C. Burla, M. Camalli, G.L. Cascarano, C. Giacovazzo, A. Guagliardi, A.G.G. Moliterni, G. Polidori, R. Spagna, J. Appl. Cryst. 32 (1999) 115–119.
[12] G.M. Sheldrick, Acta Cryst. A 64 (2008) 112–122.
[13] L.J. Farrugia, J. Appl. Cryst. 32 (1999) 837–838.
[14] J. de Meulenaar, H. Tompa, Acta Crystallogr. Sect A 19 (1965) 1014–1018.
[15] T. Miyadai, H. Mori, T. Oguchi, Y. Tazuke, H. Amitsuka, T. Kuwai, Y. Miyako, J. Magn. Magn. Mater. 104–107 (1992) 47–48.
[16] C.P. Susz, J. Muller, K. Yvon, E. Parthé, J. Less-Common Met. 71 (1980) P1–P8.
[17] I.J. Ohsugi, T. Kojima, C.B. Vining, M. Sakata, I.A. Nishida, in: Proceedings of the XVII International Conference on Thermoelectricity, 24–28 May 1998, Nagoya, Japan, pp. 370–373.
[18] J.S. Hwang, K. Lin, C. Tien, Rev. Sci. Instr. 68 (1997) 94.
[19] L.M. Gelato, E. Parthé, J. Appl. Cryst. 20 (1987) 139–143.
[20] B. Buffat, B. Chevalier, B. Czeska, J. Etourneau, J. Magn. Magn. Mater. 62 (1986) 53–56.
[21] Y.D. Seropegin, B.I. Shapiev, A.V. Gribanov, O.I. Bodak, J. Alloys Compd. 288 (1999) 147–150.
[22] C. Rizzoli, P.S. Salamakha, O.L. Sologub, O.V. Zaplatynsky, J. Alloys Compd. 385 (2004) L3–L5.
[23] L.G. Akselrud, Y.P. Yarmolyuk, I.V. Rozhdestvenskaya, E.I. Gladyshevskii, Sov. Phys. Crystallogr. 26 (1981) 103–104.
[24] S. Bobev, E.D. Bauer, F. Ronning, J.D. Thompson, J.L. Sarrao, J. Solid State Chem. 180 (2007) 2830–2837.
[25] P.T.B. Shaffer, Acta Crystallogr. B 25 (1969) 477–488.
[26] L.H. Fuchs, E. Gebert, Am. Mineral. 43 (1958) 243–248.
[27] J.A. Stepien, K. Lukaszewicz, E.I. Gladyshevskii, O.I. Bodak, Bull. Acad. Pol. Sci. (Ser. Sci. Chim.) 20 (1972) 1029–1036.
[28] V. Fritsch, S. Bobev, J.D. Thompson, J.L. Sarrao, J. Alloys Compd. 388 (2005) 28–33.
[29] P. Schobinger-Papamantellos, G. andré, J. Rodriguez-Carvajal, K.H.J. Buschow, L. Durivault, J. Alloy. Compd. 325 (2001) 29–36.
[30] G. Amoretti, J.M. Fournier, J. Magn. Magn. Mater. 43 (1984) 1217–1220.
[31] H. Ibach, H. Lüth, Solid State Physics, An introduction to Principles of Materials Science, 3rd Edition, Springer Verlag, 2003.
[32] N.F. Mott, H. Jones, The Theory of the Properties of Metals and Alloys, Oxford University Press, 1958.